Vignesh Ahilan, Michaela Wilhelm, Kurosch Rezwan

Porous polymer derived ceramic (PDC)-montmorillonite-H3PMo12O40/SiO2 composite membranes for microbial fuel cell (MFC) application

Journal Article as: peer-reviewed accepted version (Postprint)

DOI of this document*(secondary publication): https://doi.org/10.26092/elib/2489

Publication date of this document: 25/09/2023

* for better findability or for reliable citation

Recommended Citation (primary publication/Version of Record) incl. DOI:

Vignesh Ahilan, Michaela Wilhelm, Kurosch Rezwan,
Porous polymer derived ceramic (PDC)-montmorillonite-H3PMo12O40/SiO2 composite membranes for microbial fuel cell (MFC) application,
Ceramics International, Volume 44, Issue 16, 2018, Pages 19191-19199, ISSN 0272-8842,
https://doi.org/10.1016/j.ceramint.2018.07.138

Porous polymer derived ceramic (PDC)-montmorillonite-$H_3PMo_{12}O_{40}/SiO_2$ composite membranes for microbial fuel cell (MFC) application

Vignesh Ahilan, Michaela Wilhelm*, Kurosch Rezwan

University of Bremen, Advanced Ceramics, Am Biologischen Garten 2, IW3, Germany

ARTICLE INFO

Keywords:
Polymer derived ceramics (PDC)
Montmorillonite
$H_3PMo_{12}O_{40}/SiO_2$
Porosity
Ion exchange capacity
Cation transport number and oxygen mass transfer and diffusion coefficient

ABSTRACT

Ceramic membranes can serve as viable alternatives to the less mechanically stable polymeric membranes utilized in microbial fuel cells (MFCs). In this work, a series of polymer-derived ceramic (PDC) proton exchange composite membranes with large ion exchange capacity (IEC) values, high cation transport numbers, and low oxygen diffusion coefficients have been synthesized at various pyrolysis temperatures using a pressing technique. These materials were composed of a polysiloxane matrix mixed with proton-conducting fillers such as montmorillonite and $H_3PMo_{12}O_{40}/SiO_2$ at different ratios. By tuning the average pore sizes of the membranes between 0.1 and 1 μm and their hydrophilic/hydrophobic characteristics, the maximum IEC of 0.6072 mequiv/g and cation transport number of 0.6988 were obtained, which is 67% and 72% of polymeric nafion performance, respectively. In addition, the minimal oxygen mass transfer coefficient achieved by this approach was equal to 5.62×10^{-4} cm/s, which is very close to the commercial nafion membrane value. The fabricated PDC composite membranes meet all the essential criteria required for their use in MFC applications and represent a high potential to overcome limitations of polymeric membrane.

1. Introduction

Renewable energy resources have attracted much attention around the globe since it was found that the use of fossil fuels contributed to the global warming [1]. Another serious issue is the shortage of wastewater treatment facilities, which is often observed in rural areas [2]. Microbial fuel cells (MFCs) represent a possible solution to these problems due to their ability to simultaneously generate green electricity from natural resources and perform wastewater treatment using an eco-friendly approach. Generally, MFCs mimic biological electrochemical systems, in which bacteria catalyze the oxidation of wastewater inside an anaerobic anodic chamber and reduction of oxygen in an aerated cathodic chamber, which are separated by a proton conducting membrane [3–5]. The properties of this membrane strongly affect the mass transport parameters, ohmic characteristics, voltage, and electrochemical performance of the cell. Moreover, the majority of MFC designs utilize polymeric Nafion membranes because of their high proton conductivity. However, the large-scale application of this technology is limited by the relatively high costs of these membranes [6,7]. Vantanpour et al. reported that the use of sulfonated polyethersulfone polymeric membranes as the proton-conducting MFC membranes resulted in higher power density, higher chemical oxygen demand removal, and greater columbic efficiency of the cell as compared to the values obtained using commercially available Nafion membranes [8]. Nevertheless, these polymeric membranes possess low mechanical and chemical stabilities as well as high permeability for oxygen molecules [9]. In a recent study, the properties of various ceramic membranes for MFC applications (including alumina, mullite, pyrophylite, and earthenware ones) were compared [10,11], and the power densities of $6.93\,W\,m^{-3}$ and $6.85\,W\,m^{-3}$ of the resulting MFC systems were achieved using pyrophyllite and earthenware membranes, respectively. However, these values were significantly lower than the magnitudes obtained for the commercial Nafion membranes [9]. Moon et al. reported that the high resistances and low ion exchange capacities (IECs) of membranes generally decreased the current and power densities of the fabricated MFCs [12]. Furthermore, the diffusion of oxygen through the membrane deteriorated the MFC performance due to the interruption of the anaerobic conditions maintained in the anodic chamber [13]. Several research groups also found that the IEC, oxygen diffusion coefficient, and cation transport number of a membrane represent the main factors affecting the ultimate performance of the resulting MFC system [14–16].

Alternatively, a new class of ceramics derived from organosilicon systems, which is called polymer derived ceramics (PDCs), is characterized by tailored chemical compositions, enhanced surface characteristics, and micro/meso/macroporous structures [17,18]. These

* Corresponding author.
E-mail address: mwilhelm@uni-bremen.de (M. Wilhelm).

https://doi.org/10.1016/j.ceramint.2018.07.138
Received 30 May 2018; Received in revised form 13 July 2018; Accepted 14 July 2018
Available online 17 July 2018

materials can be potentially used for electrical energy storage and membrane applications including hydrogen separation, membrane filtration, and adsorption [19–21]. Since the porosity, pore size distribution, surface characteristics, and ionic conductivity as well as the mechanical and thermal stabilities of porous ceramics are directly related to their ability to perform a desired function in a particular application, these parameters must be thoroughly controlled to maximize the membrane performance [22–24]. Moreover, all these characteristics are strongly influenced by the utilized processing route, pyrolysis conditions, and additives used for producing porous ceramics [25,26]. The porosity of PDC-based ceramics can be tailored by varying the pyrolysis temperature or by adding a high surface area material (filler) and/or sacrificial template [27] to the polymer matrix. The IEC of the produced membrane depends on its selectivity and degree of permeability [28]; the former parameter can be improved by tailoring the ratio between the hydrophilic and hydrophobic interactions, while the latter is typically enhanced by using macropores [25]. However, the proton-conducting characteristics of these materials must be improved by adding various fillers to the PDC matrix, which also allows tuning the pore structure and promotes its binding ability. Nogami et al. reported that the pore size distribution of a silica material strongly influenced its proton conductivity and diffusivity since the transfer of protons across the pore surface was realized by hopping water molecules [29]. Li et al. found that porous silica tended to adsorb water molecules on its surface, which improved the proton conduction properties [30]. According to Gelir et al., the diffusion of oxygen molecules through a membrane mainly occurs in two steps, which consist of their adsorption on its surface followed by the transport through the membrane pores [31].

Ghadge et al. reported that the ceramic membranes fabricated from montmorillonite-containing red soil utilized as a proton conducting filler exhibited a higher cation transfer number and a lower oxygen diffusion coefficient as compared to those of the commercial Nafion membranes, while the maximum power density of the MFCs manufactured from these membranes yielded to $7.5\,W\,m^{-3}$ [32]. Yousefi et al. reported that a chitosan/montmorillonite composite coating on the commercial ceramic membrane acts as an oxygen barrier layer in the ceramic membrane, which improved the performance of MFC [33]. A similar approach, the incorporation of montmorillonite into polymeric Nafion membranes, increased their proton conductivities and minimized the effect of methanol crossover; the maximum power output of the resulting PEM was 122% of the magnitude obtained for the commercial Nafion 117 membrane [34]. Furthermore, composite materials consisting of heteropolyacids and SiO_2 were also used as conducting fillers for Nafion membranes. The proton conductivities of the resulting materials were one order of magnitude higher than that of the commercial Nafion membrane [35–37]. Jiang et al. found that the incorporation of various heteropolyacids into a polyether ketone matrix increased the ion exchange and water retention capacities of the produced composite membrane [38].

The objective of this work was to synthesize and characterize inexpensive porous PDC membranes for MFCs with good proton exchange properties. For this purpose, pure polysiloxane-based and composite membranes blended with different proton conducting fillers (including montmorillonite and $H_3PMo_{12}O_{40}/SiO_2$ (PMA)) were fabricated by simple pressing and pyrolysis techniques. The functional properties of the as-prepared membranes were evaluated inside a dual chamber tank, and their oxygen diffusion coefficients, mass transfer coefficients, and cation transport numbers were determined and compared with those of the commercial polymeric Nafion 117 membrane examined under the same conditions.

2. Materials and methods

2.1. Chemicals

Commercial hydrophobic oligomeric methyl-phenyl polysiloxane powder (Silres® H44, Wacker Chemie AG), monomeric aminopropyltriethoxysilane (APTES, ABCR Dr. Braunagel GmbH & Co. KG), montmorillonite K10 (Sigma Aldrich), phosphomolybdenic acid hydrate ($H_3PMo_{12}O_{40}\ xH_2O$, Alfa Aesar), tetraethylorthosilicate (TEOS, Sigma Aldrich), ethanol solvent, ammonia solution, and water were used for membrane preparation.

2.2. Preparation of PMA filler

The filler material was prepared using a method previously developed by Li et al. [39] with minor modifications. First, 1.99 g of quaternary dodecyltrimethylammonium chloride was dissolved in 200 mL of 2.5 M HCl aqueous solution in a 250-mL conical flask followed by the addition of 17.83 mL of TEOS and 4.69 g of $H_3PMo_{12}O_{40}{\cdot}H_2O$ under stirring at a speed of 800 rpm for 1 h. After that, the mixture was aged at room temperature for 4 h, separated by filtration, thoroughly washed with ethanol, and dried inside an oven at a temperature of 80 °C for 24 h.

2.3. Synthesis of PDC membranes

A scheme of the utilized synthesis procedure is shown in Fig. 1a. The as-prepared PMA composite or montmorillonite filler was dispersed in ethanol for 30 min via ultrasonication followed by the addition of a mixture of H44 and APTES with the subsequent polymerization for 3 days under reflux at a temperature of 70 °C (a solution containing 3.27 mL of NH_3 in 3 mL of water was used as a catalyst). After removing the solvent, drying, cross-linking in air at 200 °C for 2 h, and grinding using a high-energy ball mill, the resulting fine powder was pressed to a monolithic membrane. The fabricated membranes were pyrolyzed at temperatures of 400, 500, 600, and 1000 °C under nitrogen atmosphere (see Fig. 1b). The material compositions and the sample nomenclature are shown in Table 1.

2.4. Material characterization

The X-ray diffraction (XRD) pattern of the samples was measured using SEIFERT XRD 3003 research edition, United States. The Fourier Transform Infrared spectroscopy (FTIR) was measured using Bruker equinox 55 with ATR unit. The surface morphology of the samples was carried out by means of scanning electron microscopy (SEM, Camscan Series 2, Obducat CamScan Ltd, 20 kV). The macroporosity of the membranes was analyzed using mercury intrusion porosimetry (Pascal 140/440, POROTEC GmbH). The micro and mesoporosity, as well as the resulting specific BET surface areas, were determined by nitrogen adsorption/desorption isotherms at −196 °C (Belsorp-Mini, Bel Japan Inc.). The samples were degassed at 120 °C for 3 h as a pretreatment in order to remove water molecules adsorbed on the surface of the material. The surface characteristics of the materials were analyzed by placing the 0.5 g of dried PDC powder composite material inside a closed Erlenmeyer flask filled with the solvent (water or heptane, respectively) in equilibrium with its vapor phase at room temperature. Samples were weighed at the start and end of a 24 h measurement period in order to determine the vapor adsorption of the material. Later, the adsorption of solvent was recalculated into $mmol/m^2$ using the BET specific surface of the materials.

2.5. Ion exchange capacity

The ion exchange capacity of the membrane was calculated using titration method, firstly the membrane was equilibrated with 100 mL of

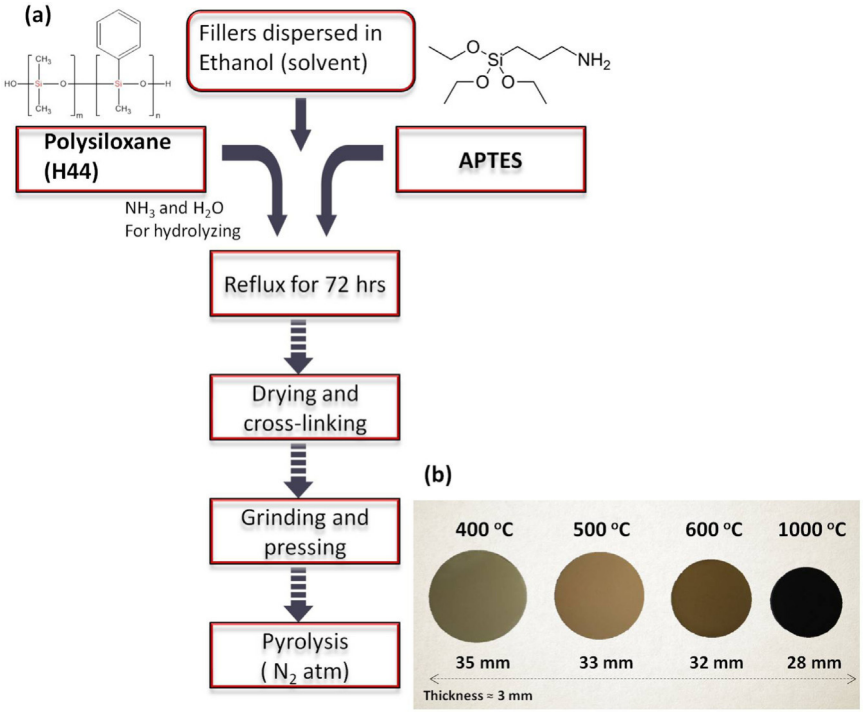

Fig. 1. (a) Process scheme of PDC membranes (b) synthesized PDC membranes at different pyrolysis temperature.

1 M HCl solution for 72 h. After that they were removed from the acid solution and rinsed with D.I water in order to remove the surface adsorbed ions on the membranes. Then they were transferred to 50 mL of 1 M NaCl to exchange the H^+ to Na^+ ions equilibrated for 24 h. After that, the membrane was removed and the NaCl solution was titrated with 0.005 M of NaOH giving the amount of H^+ ions present in the solution. The IEC was expressed in milliequivalents of H^+ per gram of dry membrane using Eq. (1).

$$IEC = (V_{NaOH} x M_{NaOH})/W_{dry} \quad (1)$$

V_{NaOH} – volume of NaOH solution consumed
M_{NaOH} – molarity of NaOH (0.005 M)
W_{dry} – weight of dry sample

2.6. Cation transport number

Cation transport number (t_+) were evaluated using the double chamber tank, where the anode chamber is filled with 0.5 M NaCl solution and cathode chamber with 0.005 M NaCl solution to create an osmotic drag concentration gradient. Two identical Ag/AgCl reference electrodes were used to measure the potential difference between the closest point of both sides of the membrane and to monitor the potential difference with respect to time. The t_+ value was calculated using Eq. (2)

$$E_v = RT/F(2t-1)\ln(C_1/C_2) \quad (2)$$

E_v – potential difference at the nearest point of the membrane (mV)
R – gas constant
F – Faraday constant (C mol^{-1})
T – temperature (°K)
t – cation transport number
C_1 – anode chamber concentration (0.5 M)
C_2 – cathode chamber concentration (0.005 M)

2.7. Oxygen diffusion coefficient

The D.I water filled anodic chamber was continuously purged with N_2 gas for 30 min and maintain the anode chamber in the anaerobic state with oxygen concentration less than 0.02 mg/l, whereas the D.I water filled cathodic chamber aerated continuously to maintain the dissolved oxygen condition closed to saturation. The oxygen concentration in the anodic chamber was continuously monitored using DO probe at regular interval of 15 min and oxygen mass transfer and diffusion coefficient were calculated using the Eqs. (3) and (4), respectively.

$$K_o = -v/At\ln(C_{oc} - C_{oa})/C_{oc} \quad (3)$$

$$D_o = K_o * L_{th} \quad (4)$$

K_o – oxygen mass transfer coefficient (cm/s)
D_o – oxygen diffusion coefficient (cm^2/s)
v – volume of the chamber (cm^3)
A – area of the membrane (cm^2)
t – time (s)
C_{oc} – oxygen concentration in cathode
C_{oa} – oxygen concentration in anode
L_{th} – thickness of the membrane

Table 1
Prepared membranes, their composition and pyrolysis parameters.

Samples	H44 (mol)	APTES (mol)	Montmorillonite (wt%)	$H_3PMo_{12}O_{40}/SiO_2$ (wt%)	Temperature (°C)
PDC	1	1	0	0	400/500/600/1000
PDC:M20	1	1	20	0	400/500/600/1000
PDC:PMA10:M10	1	1	10	10	400/500/600

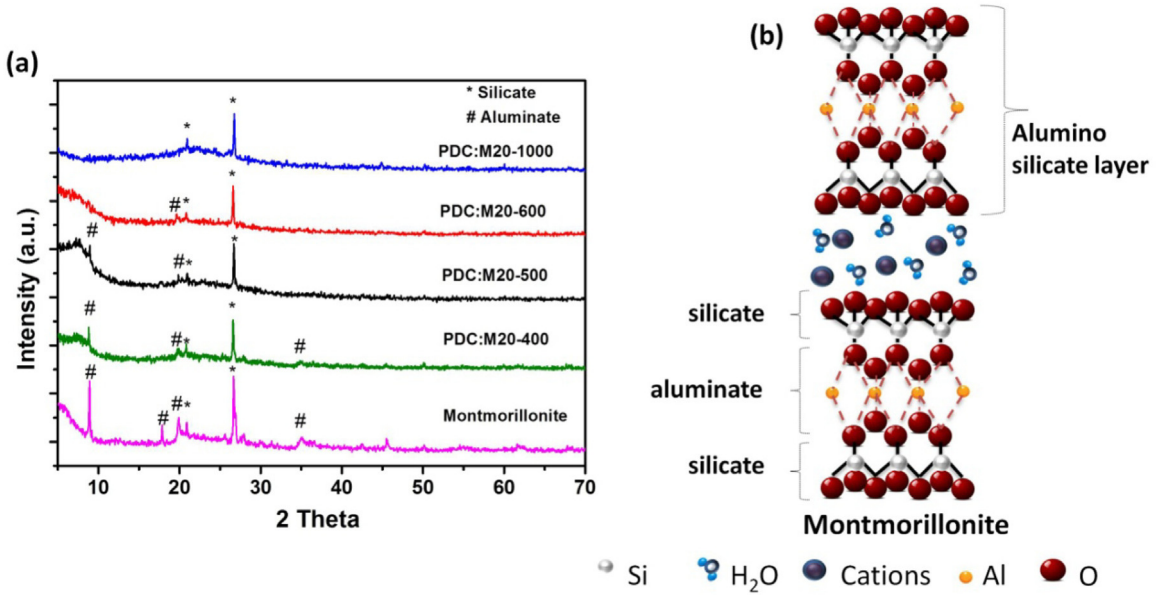

Fig. 2. (a) XRD image of PDC:M20 based membranes with respect to pyrolysis temperature (b) structure of montmorillonite clay mineral.

3. Results and discussion

3.1. Phase analysis

X-ray diffraction (XRD) patterns of the prepared membranes were recorded to analyse their crystalline phases obtained at different pyrolysis temperatures as shown in Fig. 2a. The XRD pattern of the montmorillonite K10 mineral indicates that it belongs to the smectite group of aluminosilicates containing some impurities such as quartz, cristobalite, and feldspar, as previously reported in detail by Varadwaj et al. [40]. Fig. 2a demonstrates that the membranes formed at 400 and 500 °C have the stable structure of a smectite mineral. When the temperature was further increased to 600 °C and 1000 °C, partial and complete decompositions of this structure were observed, respectively, followed by the formation of a stable silicate phase. The layered smectite structure contains aluminate and silicate species with interlayer spacing [41], as shown in Fig. 2b. The obtained XRD patterns reveal that PDC-based materials are amorphous in nature due to the presence of amorphous carbon and silica in the Si–O–C matrix (even at the pyrolysis at a high temperature of 1000 °C). The amorphous structure of Si–O–C is composed of tetrahedrally coordinated $SiO_{4-x}C_x$ (x = 1–4) structural units containing SiO_2- and C-enriched regions, as previously observed by other research groups [42,43]. In a similar way, the XRD patterns of the PDC:PMA10:M10 based materials show that the SiOC matrix and PMA filler are amorphous compounds, whereas the montmorillonite phase still retains its crystalline structure (see Supporting information Fig. S1). Zhao et al. found that the addition of SiO_2 filler increased the thermal stability of the $H_3PMo_{12}O_{40}$ structure in the temperature region up to 550 °C [39]. The FTIR spectrum of PMA is displayed in Fig. S2. It shows the four characteristic bands between 1100 and 700 cm^{-1} (indicating the presence of a Keggin-type structure) that are centered at 1079 cm^{-1} (P–O stretching in the central PO_4 tetrahedron), 957 cm^{-1} (terminal Mo=O groups of the exterior MoO_6 octahedron), 881 cm^{-1}, and 796 cm^{-1} (Mo–O_b–Mo and Mo–O_c–Mo bridges, respectively). Fig. S3 visualizes the surface morphology of PDC-1000 membrane and indicates that this ceramic membrane is porous in nature. This porous nature of the ceramics improves the efficiency of proton transfer through the membrane in the MFC system.

3.2. Porosity and pore size distribution

The pore sizes of the prepared membranes determined by an Hg intrusion technique varied from 0.1 to 1 μm, while their degrees of porosity ranged from 25% to 40% depending on the pyrolysis temperature and filler composition (see Fig. 3a–c). The average pore sizes of the pure PDC membranes decrease with decreasing particle size of the pre-pyrolyzed material, as shown in Table S1. Moreover, the pore size of the membrane first increases with increasing pyrolysis temperature to 600 °C, but then decreases at a higher pyrolysis temperature of 1000 °C. This phenomenon is often attributed to the shrinkage of particles and decomposition of organic molecules present in the polysiloxane matrix [27,44]. The PDC:M20–400 membrane exhibits an average pore size of 410 nm, which is smaller than that of the PDC-400 membrane (620 nm) due to the smaller particle size distribution of PDC:M20 pre-pyrolyzed powder. On the other hand, the PDC:PMA10:M10–400 based material has an average pore size of 260 nm, which is much lower than those of the other PDC membranes, owing to the further addition of PMA filler, which decreases the average particle size of the pre-pyrolyzed membrane. In addition, the formation of mesopores (x = 2–50 nm) was observed for the PDC:PMA10:M10 based membranes, but not for the bare PDC and PDC:M20 ones due to the presence of micro- and mesopores in the PMA structure. The membranes containing macropores with sizes as high as 250 nm are most suitable for MFC applications because of their limited oxygen permeability and good ionic transport properties. Similarly, Li et al. concluded that the performance of porous membranes for MFCs was strongly dependent on their oxygen transfer, cation transfer, and proton diffusion characteristics, which drastically affected the columbic efficiency and power density of the resulting MFC systems [45]. A porous ceramic membrane promotes proton transfer due to its high porosity rather than good ionic conductivity, as previously observed by Winfield et al. [46].

3.3. Specific surface area

N_2 adsorption/desorption isotherms were obtained to identify the type of the membrane pore structure and determine its specific surface area. Fig. 4a–b show the Brunauer–Emmett–Teller (BET) isotherms recorded for all the as-prepared PDC materials. The PDC and PDC:M20 based membranes pyrolyzed at 400, 500, and 600 °C exhibit type I

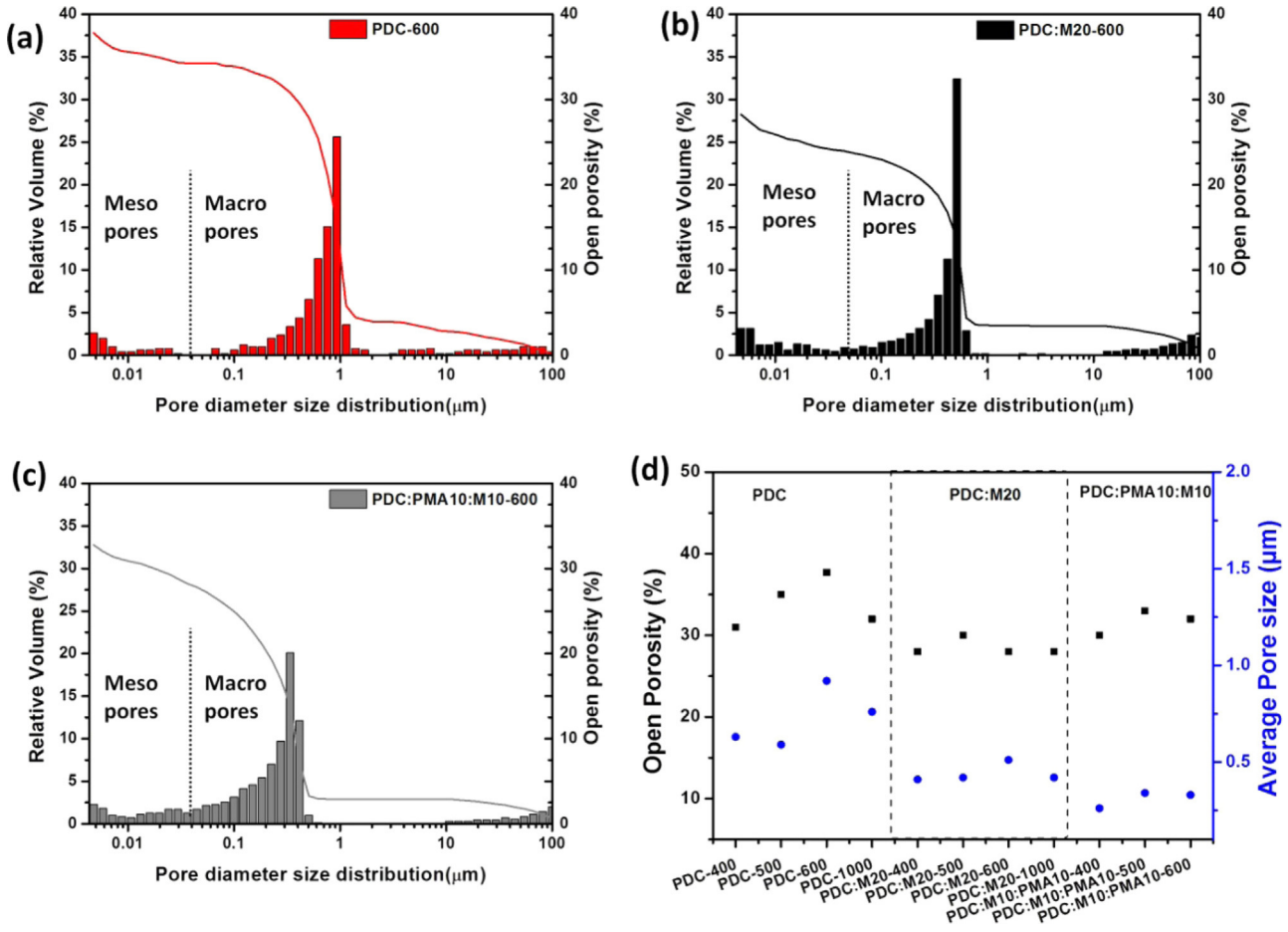

Fig. 3. (a–c) Pore size distribution versus relative pore volume and open porosity curves obtained from Hg-porosimetry histogram of pyrolyzed samples (d) average pore size and open porosity versus as prepared PDC membrane plots.

isotherms typical for microporous structures (according to the classification of the International Union of Pure and Applied Chemistry). The sample pyrolyzed at 1000 °C has no micropores, and its specific surface area is low because of the collapse of pores caused by the viscous flow at pyrolysis temperatures greater than 500 °C [47]. The surface area of the PDC-400 material is about 2.5 m^2/g, whereas that of PDC:M20–400 equals 112 m^2/g, which can be explained by the presence of the layered montmorillonite structure in the PDC matrix (the surface area of pure montmorillonite is 250 m^2/g). After pyrolyzing the montmorillonite-functionalized PDC material at 500 °C, its surface area increased to 428.83 m^2/g. The further increase in the pyrolysis temperature to 600 °C slightly lowered the surface area due to the partial decomposition of the montmorillonite structure, as confirmed by the XRD spectra. On the other hand, the surface area of the PDC material functionalized with both montmorillonite and PMA ranged between 88 and 300 m^2/g at pyrolysis temperatures from 400 to 600 °C due to the presence of microporous and mesoporous structures identified by the type IV isotherms depicted in Fig. 4c. Between 500 and 600 °C, the PMA filler starts to decompose simultaneously with the PDC matrix, leading to a slight decrease in the surface area.

PDC and its composites typically contain micro-, meso-, and macropores, which strongly influence the proton transfer properties of the produced membranes. Xu et al. reported that the presence of mesopores in a material enhanced its proton conduction characteristics as compared to those of non-porous membranes [48]. However, the formation of highly ordered narrow pores also increases the flux of water molecules and promotes the diffusion of oxygen species, which negatively affects the long-term performance of MFC systems. Since the ceramic membranes produced in this work contain a mixture of micro/meso- and macropores in the SiOC structure, they represent a potential solution to these problems. The smooth surface characterized by irregular or non-linear pores that decrease the permeability of oxygen gas and water from one chamber of the MFC system to another exhibits good diffusion properties [49].

3.4. Surface characteristics (hydrophilicity/hydrophobicity)

The surface characteristics of the prepared membrane materials for MFC applications (including their degrees of hydrophilicity) were analyzed by n-heptane and water vapor adsorption methods, and the obtained results are shown in Fig. 5a. The amounts of adsorbed vapors (in mmol m^{-2}) were determined from the changes in the specific surface area measured by recording N_2 adsorption-desorption isotherms. When the water/heptane ratio is higher than one, the studied material is assumed to possess hydrophilic properties (see Fig. 5b). The PDC-based materials exhibit a higher degree of hydrophilicity with increasing pyrolysis temperature due to the decomposition of the hydrophobic methyl and phenyl groups of the polysiloxane (H44) matrix [50]. Prenzel et al. found that increasing the APTES content in the polysiloxane precursor made the final pyrolised PDC material more hydrophilic due to the lower temperature stability of the propylamino chains of the APTES groups [51]. The water/heptane ratio slightly decreased after the functionalization of the synthesized PDC materials with montmorillonite, due to its hydrophobic nature [52,53]. However, its ratio greater than one were obtained for PDC:M20–600 and PDC:M20–1000, while their degrees of hydrophilicity were smaller than those of the PDC-based materials. The PDC:PMA10:M10 material exhibited a similar hydrophilic nature, while the samples pyrolyzed at

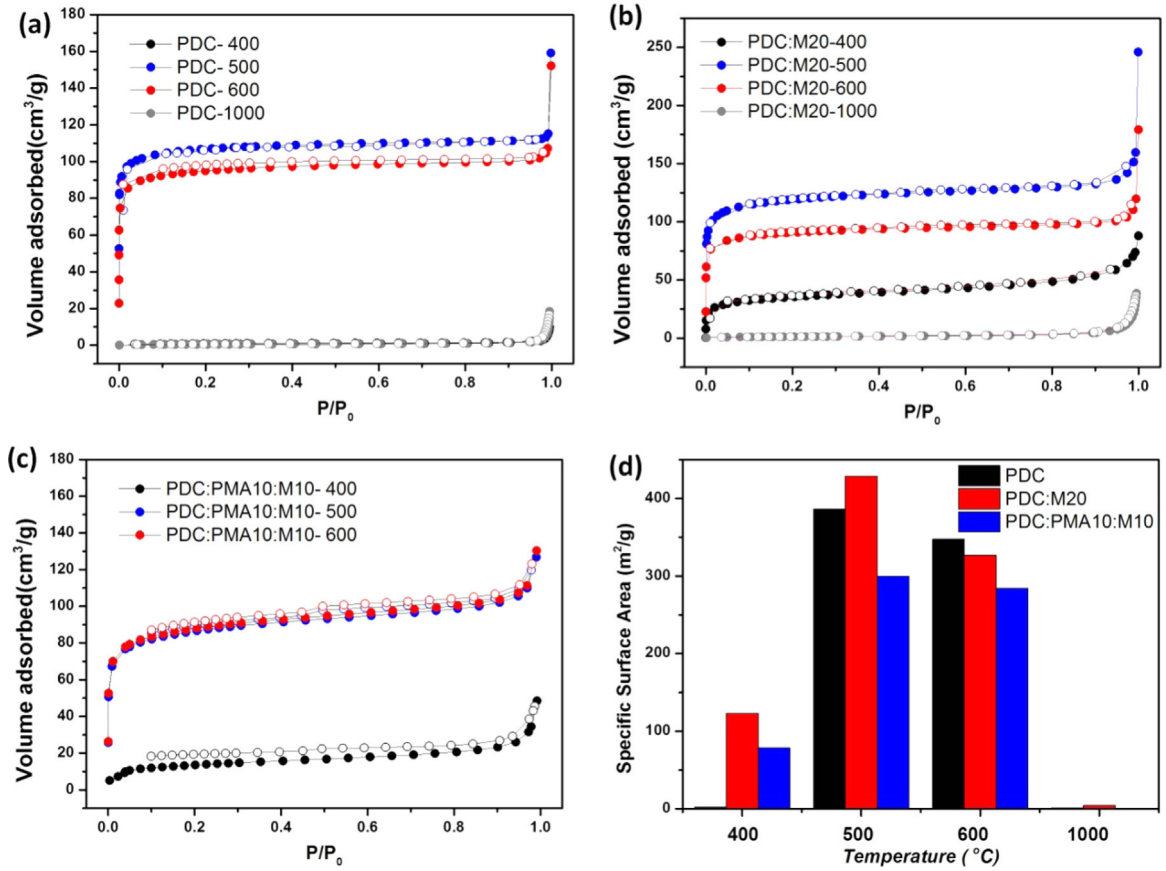

Fig. 4. (a–c) Nitrogen adsorption desorption isotherms of PDC and composite membranes, pyrolyzed at 400, 500, 600 and 1000 °C (d) specific surface areas of pyrolyzed (400/500/600/1000 °C) membranes as determined by nitrogen adsorption isotherm.

500 °C and 600 °C were characterized by the highest water/heptane ratios as compared to those of the other specimens due to the alignment of the Keggin $H_3PMo_{12}O_{40}$ structure. The utilized filler possessed the ability to retain water molecules inside its micro- and mesopores, which was consistent with the types of the N_2 adsorption isotherms recorded.

3.5. Ion exchange capacity

The IEC values (Fig. 6a) of the PDC:M20 based materials obtained using a back titration method were higher than those measured for the PDC-based materials. In contrast, the IEC of the sample pyrolyzed at 1000 °C was relatively low because of the decomposition of its layered montmorillonite structure containing aluminates and silicates. Moreover, for the PDC:M20–600 sample, a dramatic increase in IEC value was observed as compared to that of the PDC-600 sample due to the existence of the montmorillonite structure with negative charges. On the other hand, the specimens containing montmorillonite and PMA fillers exhibited a tremendous increase in IEC after the pyrolysis at 400 °C and 500 °C, whereas the PDC:PMA10:M10–600 membrane showed a drop in IEC as compared to the values obtained for the PDC-600 and PDC:M-20–600 samples, owing to the thermal instability of the PMA filler. The IEC magnitudes of the PDC:PMA10:M10–400 and

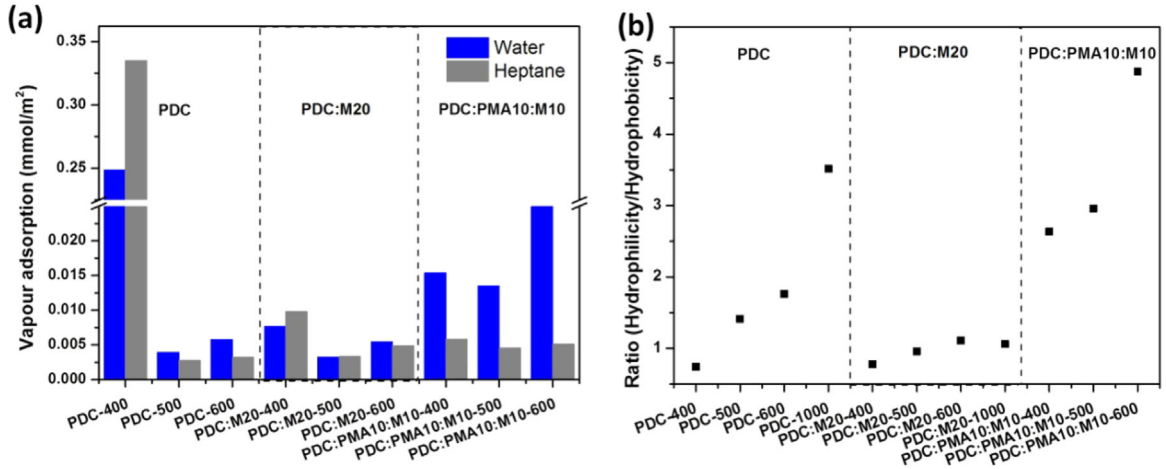

Fig. 5. (a) Water and n-heptane vapor adsorption at 25 °C for as prepared membrane materials (b) ratio of hydrophilic and hydrophobic nature for all membranes as prepared.

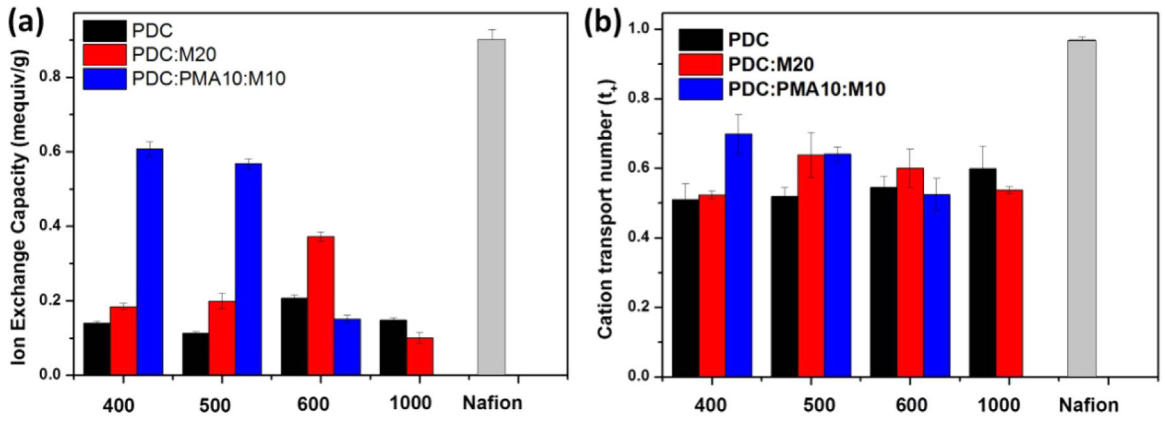

Fig. 6. (a) Ion exchange capacity measured for as prepared ceramic membrane compared with nafion (b) cation transport number of ceramic membrane compared with nafion.

PDC:PMA10:M10–500 membranes were five and six times higher than those of the PDC-500 and PDC-400 samples, respectively, and were equal to almost 68% of the IEC of the polymeric Nafion membrane. The ion transfer in ceramic membranes is realized via the hopping of protons between the hydroxyl groups and water molecules adsorbed on the porous PDC surface, whereas the addition of montmorillonite and PMA fillers facilitates the transfer of protons by the presence of charged ions in their structures [54].

3.6. Cation transport number

The functionalization of PDC with montmorillonite slightly increases its cation transport number (Fig. 6b) as compared to those of the bare PDC and PDC:M20 materials pyrolyzed at 400, 500, and 600 °C. At a pyrolysis temperature of 1000 °C, its magnitude decreases due to the complete decomposition of the aluminate layer in the montmorillonite structure. In addition, the presence of micro- and mesopores in the membrane provides better pathways for the diffusion of ions from one chamber to another. Many researchers concluded that the diffusion of ions through porous membranes represented a classical problem of diffusion chemistry [46,48]. The presence of SiOC species in the montmorillonite structure along with aluminate and silicate species leads to optimal surface characteristic for MFC applications, which are also assumed to promote the diffusion of ions through the membrane body. The adsorption of water molecules on the ceramic surface is enhanced by the negatively charged sites of the layered montmorillonite structure, which promotes the ion transfer from one MFC chamber to another. The PDC:PMA10:M10 based membrane exhibits a higher cation transport number as compared to those of the other membranes, due to the incorporation of PMA filler into the Keggin structure. According to Wang et al., this material possesses the ability to retain water molecules in its mesoporous structure and acts as a proton-conducting filler even for polymeric Nafion-based membranes [55]. The higher cation transport number obtained for the sample pyrolyzed at 400 °C resulted from the alignment of the Keggin shape and mesoporous structure of the PMA filler. However, PMA decomposes at temperatures above 550 °C (even under inert atmosphere), leading to a sharp decrease in the cation transfer number of the PDC:PMA10:M10–600 sample. The destruction of the PMA Keggin structure observed at 600 °C and the beginning of the transformation of the alpha-MoO_3 phase decreased the number of mesopores and thus negatively affected its water-retaining ability [39]. The cation transport number of the composite membrane with montmorillonite and PMA fillers pyrolyzed at 400 °C is equal to 72% of that of the polymeric Nafion membrane, which represents a relatively high value for MFC ceramic membranes. This phenomenon can be attributed to the smallest average pore size (260 nm) and highly hydrophilic surface of this membrane, which presumably promote the transfer of protons via a proton hopping mechanism, as previously reported by Nogami et al. [29].

3.7. Diffusion of dissolved oxygen

One of the major purposes of using membranes in MFCs is to prevent the leakage of oxygen molecules from the aerobic cathode chamber to the anode chamber and maintain its anaerobic conditions. In this work, the diffusion of dissolved oxygen species through the PDC membranes was compared with their diffusion through the commercial polymeric Nafion membrane. This process can be suppressed by tailoring the average membrane pore size since its degree of porosity strongly affects the oxygen diffusion coefficient [45]. The PDC-600 membrane exhibits a degree of porosity and an average pore size of 920 nm. These values are higher than the values obtained for the other membranes synthesized in this study. As a result, its oxygen diffusion coefficient of 7.06×10^{-4} cm^2/s is noticeably higher than that of the PDC:M20–600 membrane (6.86×10^{-4} cm^2/s), owing to the presence of montmorillonite in the SiOC matrix, which decreases its porosity degree to 28% and to an average pore size of 510 nm. The pyrolysis temperature also produces a significant effect on the degree of porosity and average pore size of the membrane that decreases the amount of diffused oxygen. For instance, the diffusion coefficient of dissolved oxygen obtained for the PDC-400 membrane is 2.41×10^{-4} cm^2/s, and that of the material pyrolyzed at 1000 °C (PDC–1000) is equal to 1.93×10^{-4} cm^2/s due to the increase in porosity and average pore size of the ceramic membrane with increasing pyrolysis temperature. On the other hand, the PDC:PMA10:M10 based membrane pyrolyzed at 500 °C is characterized by the smallest oxygen diffusion coefficient of 1.68×10^{-4} cm^2/s (as compared to those of the PDC and PDC:M20 based membranes), owing to the changes in the average pore size and degree of porosity as well as the presence of the PMA Keggin structure. The mass transfer coefficient of dissolved oxygen through the polymeric Nafion membrane is equal to 3.06×10^{-4} cm/s, which is very close to the value of 5.45×10^{-4} cm/s obtained for the PDC:PMA10:M10–500 membrane in this work. The oxygen diffusion coefficient mainly depends on the membrane thickness; therefore, its value determined for the thin polymeric Nafion 117 membrane (with a thickness of 170 μm) was 2 orders of magnitude smaller than those of the ceramic membranes with thicknesses of 3–4 mm. The oxygen mass transfer and diffusion coefficients of the membranes prepared in this work are listed in Table 2.

4. Conclusion

In this study, PDC composite membranes were synthesized from polysiloxane precursor mixed with the montmorillonite and PMA

Table 2
Physical characterization of as prepared PDC and composite ceramic membranes.

Membranes	K_O (cm/s)	D_O (cm^2/s)	t_+	IEC (mequiv/g)	Pore size (nm)
PDC–400	7.56×10^{-4}	2.41×10^{-4}	0.5104	0.1402	630
PDC–500	7.21×10^{-4}	2.23×10^{-4}	0.5185	0.1131	590
PDC–600	7.06×10^{-4}	2.11×10^{-4}	0.5447	0.2068	920
PDC–1000	7.15×10^{-4}	1.93×10^{-4}	0.5985	0.1483	760
PDC:M20–400	5.54×10^{-4}	1.77×10^{-4}	0.5233	0.1844	410
PDC:M20–500	5.23×10^{-4}	1.50×10^{-4}	0.6378	0.1989	420
PDC:M20–600	6.86×10^{-4}	2.18×10^{-4}	0.5999	0.3723	510
PDC:M20–1000	8.20×10^{-4}	1.97×10^{-4}	0.5371	0.1006	420
PDC:M10:PMA10–400	5.62×10^{-4}	1.79×10^{-4}	0.6988	0.6072	260
PDC:M10:PMA10–500	5.45×10^{-4}	1.68×10^{-4}	0.6405	0.5686	340
PDC:M10:PMA10–600	6.88×10^{-4}	2.06×10^{-4}	0.5234	0.1516	330
Nafion	3.06×10^{-4}	5.45×10^{-6}	0.9680	0.9026	–

proton-conducting filler materials, and their IEC values, cation transport numbers, oxygen mass transfer coefficients, and diffusion coefficients were determined. The obtained results revealed that the PDC:M20–600 and PDC:PMA10:M10–400 based membranes exhibited better performances as compared to those of the other PDC membranes, while the IEC value and cation transport number of PDC:PMA10:M10–400 were equal to 67% and 68% of the magnitudes obtained for the commercial polymeric Nafion membrane, respectively. Similarly, a small oxygen diffusion coefficient of 1.79×10^{-4} cm^2/s was observed at an average membrane pore size of 260 nm, which was very close to that of the Nafion 117 membrane. Therefore, the as-prepared PDC composite ceramic membranes can be potentially utilized as the separators in MFC systems. Testing the real-scale performance and wastewater treatment efficiency of the MFCs fabricated from PDC composite membranes will be conducted in future studies.

Acknowledgement

We thank the German Federal Ministry of Education and Research (BMBF) through grant no. 01DQ15013, INNO INDIGO Partnership Program and Research Training Group “Micro-, meso- and macroporous nonmetallic Materials: Fundamentals and Applications” (MIMENIMA) through grant no. GRK 1860 for financial support.

Appendix A. Supplementary material

Supplementary data associated with this article can be found in the online version at doi:10.1016/j.ceramint.2018.07.138.

References

[1] S. Chu, Y. Cui, N. Liu, The path towards sustainable energy, Nat. Mater. 16 (2017) 16–22.
[2] T. Hey, N. Bajraktari, Å. Davidsson, J. Vogel, H.T. Madsen, C. Hélix-Nielsen, J.l.C. Jansen, K. Jönsson, Evaluation of direct membrane filtration and direct forward osmosis as concepts for compact and energy-positive municipal wastewater treatment, Environ. Technol. (2017) 1–13.
[3] C. Santoro, C. Arbizzani, B. Erable, I. Ieropoulos, Microbial fuel cells: from fundamentals to applications. A review, J. Power Sources 356 (2017) 225–244.
[4] J.R. Trapero, L. Horcajada, J.J. Linares, J. Lobato, Is microbial fuel cell technology ready? An economic answer towards industrial commercialization, Appl. Energy 185 (2017) 698–707.
[5] R. Kumar, L. Singh, A. Zularisam, F.I. Hai, Microbial fuel cell is emerging as a versatile technology: a review on its possible applications, challenges and strategies to improve the performances, Int. J. Energy Res. (2017).
[6] S. Angioni, L. Millia, G. Bruni, D. Ravelli, P. Mustarelli, E. Quartarone, Novel composite polybenzimidazole-based proton exchange membranes as efficient and sustainable separators for microbial fuel cells, J. Power Sources 348 (2017) 57–65.
[7] A. Sivasankaran, D. Sangeetha, Y.-H. Ahn, Nanocomposite membranes based on sulfonated polystyrene ethylene butylene polystyrene (SSEBS) and sulfonated SiO_2 for microbial fuel cell application, Chem. Eng. J. 289 (2016) 442–451.
[8] S. Zinadini, A. Zinatizadeh, M. Rahimi, V. Vatanpour, Z. Rahimi, High power generation and COD removal in a microbial fuel cell operated by a novel sulfonated PES/PES blend proton exchange membrane, Energy 125 (2017) 427–438.
[9] G. Pasternak, J. Greenman, I. Ieropoulos, Comprehensive study on ceramic membranes for low-cost microbial fuel cells, ChemSusChem 9 (2016) 88–96.
[10] V. Yousefi, D. Mohebbi-Kalhori, A. Samimi, Ceramic-based microbial fuel cells (MFCs): a review, Int. J. Hydrog. Energy 42 (2017) 1672–1690.
[11] J. Chouler, I. Bentley, F. Vaz, A. O'Fee, P.J. Cameron, M. Di Lorenzo, Exploring the use of cost-effective membrane materials for microbial fuel cell based sensors, Electrochim. Acta 231 (2017) 319–326.
[12] E. Ji, H. Moon, J. Piao, P.T. Ha, J. An, D. Kim, J.-J. Woo, Y. Lee, S.-H. Moon, B.E. Rittmann, Interface resistances of anion exchange membranes in microbial fuel cells with low ionic strength, Biosens. Bioelectron. 26 (2011) 3266–3271.
[13] B. Min, S. Cheng, B.E. Logan, Electricity generation using membrane and salt bridge microbial fuel cells, Water Res. 39 (2005) 1675–1686.
[14] D. Huang, B.-Y. Song, Y.-L. He, Q. Ren, S. Yao, Cations diffusion in Nafion117 membrane of microbial fuel cells, Electrochim. Acta (2017) 654–663.
[15] S. Cheng, H. Liu, B.E. Logan, Increased performance of single-chamber microbial fuel cells using an improved cathode structure, Electrochem. Commun. 8 (2006) 489–494.
[16] J.X. Leong, W.R.W. Daud, M. Ghasemi, K.B. Liew, M. Ismail, Ion exchange membranes as separators in microbial fuel cells for bioenergy conversion: a comprehensive review, Renew. Sustain. Energy Rev. 28 (2013) 575–587.
[17] P. Colombo, G. Mera, R. Riedel, G.D. Soraru, Polymer-derived ceramics: 40 years of research and innovation in advanced ceramics, J. Am. Ceram. Soc. 93 (2010) 1805–1837.
[18] A. Strachota, M. Černý, Z. Chlup, K. Depa, M. Šlouf, Z. Sucharda, Foaming of polysiloxane resins with ethanol: a new route to pyrolytic macrocellular SiOC foams, Ceram. Int. 41 (2015) 13561–13571.
[19] E. Passalacqua, S. Freni, F. Barone, Alkali resistance of tape-cast SiC porous ceramic membranes, Mater. Lett. 34 (1998) 257–262.
[20] A. Karakuscu, A. Ponzoni, P.R. Aravind, G. Sberveglieri, G.D. Soraru, Gas sensing behavior of mesoporous SiOC glasses, J. Am. Ceram. Soc. 96 (2013) 2366–2369.
[21] F. Guo, D. Su, Y. Liu, J. Wang, X. Yan, J. Chen, S. Chen, High acid resistant SiOC ceramic membranes for wastewater treatment, Ceram. Int. (2018) 13444–13448.
[22] P. Colombo, E. Bernardo, Macro-and micro-cellular porous ceramics from preceramic polymers, Compos. Sci. Technol. 63 (2003) 2353–2359.
[23] J.-H. Eom, Y.-W. Kim, I.-H. Song, H.-D. Kim, Processing and properties of polysiloxane-derived porous silicon carbide ceramics using hollow microspheres as templates, J. Eur. Ceram. Soc. 28 (2008) 1029–1035.
[24] C. Vakifahmetoglu, I. Menapace, A. Hirsch, L. Biasetto, R. Hauser, R. Riedel, P. Colombo, Highly porous macro-and micro-cellular ceramics from a polysilazane precursor, Ceram. Int. 35 (2009) 3281–3290.
[25] T. Prenzel, M. Wilhelm, K. Rezwan, Pyrolyzed polysiloxane membranes with tailorable hydrophobicity, porosity and high specific surface area, Microporous Mesoporous Mater. 169 (2013) 160–167.
[26] F. Schlüter, M. Wilhelm, K. Rezwan, Surfactant assisted syntheses of monolithic hybrid ceramics with hierarchical porosity, J. Eur. Ceram. Soc. 35 (2015) 2963–2972.
[27] P. Colombo, Engineering porosity in polymer-derived ceramics, J. Eur. Ceram. Soc. 28 (2008) 1389–1395.
[28] H.P. Gregor, Ion-exchange membranes-correlation between structure and function, Pure Appl. Chem. 16 (1968) 329–350.
[29] Y. Daiko, T. Kasuga, M. Nogami, Pore size effect on proton transfer in sol–gel porous silica glasses, Microporous Mesoporous Mater. 69 (2004) 149–155.
[30] H. Li, M. Nogami, Pore-controlled proton conducting silica films, Adv. Mater. 14 (2002) 912–914.
[31] A. Gelir, Ö. Yargı, S.A. Yüksel, Elucidation of the pore size and temperature dependence of the oxygen diffusion into porous silicon, Thin Solid Films (2017) 602–607.
[32] A.N. Ghadge, M. Ghangrekar, Development of low cost ceramic separator using mineral cation exchanger to enhance performance of microbial fuel cells, Electrochim. Acta 166 (2015) 320–328.
[33] V. Yousefi, D. Mohebbi-Kalhori, A. Samimi, Application of layer-by-layer assembled chitosan/montmorillonite nanocomposite as oxygen barrier film over the ceramic separator of the microbial fuel cell, Electrochim. Acta (2018) 234–247.
[34] M.M. Hasani-Sadrabadi, E. Dashtimoghadam, F.S. Majedi, K. Kabiri, M. Solati-Hashjin, H. Moaddel, Novel nanocomposite proton exchange membranes based on Nafion® and AMPS-modified montmorillonite for fuel cell applications, J. Membr. Sci. 365 (2010) 286–293.
[35] P. Gómez-Romero, J.A. Asensio, S. Borrós, Hybrid proton-conducting membranes for polymer electrolyte fuel cells: phosphomolybdic acid doped poly (2, 5-benzimidazole)—(ABPBI-$H_3PMo_{12}O_{40}$), Electrochim. Acta 50 (2005) 4715–4720.
[36] K. Checkiewicz, G. Żukowska, W. Wieczorek, Synthesis and characterization of the proton-conducting gels based on PVdF and PMMA matrixes doped with heteropolyacids, Chem. Mater. 13 (2001) 379–384.
[37] L.-p. Fan, L.-l. Zhang, Effect of heteropolyacid and heteropolyacid salt on the performance of nanometer proton membrane microbial fuel cell, Int. J. Electrochem. Sci. 12 (2017) 699–709.
[38] H. Wu, X. Shen, Y. Cao, Z. Li, Z. Jiang, Composite proton conductive membranes composed of sulfonated poly(ether ether ketone) and phosphotungstic acid-loaded imidazole microcapsules as acid reservoirs, J. Membr. Sci. 451 (2014) 74–84.
[39] S. Li, J. Zheng, W. Yang, Y. Zhao, Preparation and characterization of 3DOM $H_3PMo_{12}O_{40}$–SiO_2 with Keggin structure, Chem. Lett. 36 (2007) 758–759.
[40] G.B.B. Varadwaj, S. Rana, K. Parida, Amine functionalized K10 montmorillonite: a solid acid–base catalyst for the Knoevenagel condensation reaction, Dalton Trans. 42 (2013) 5122–5129.

[41] S. Ng, J. Plank, Interaction mechanisms between Na montmorillonite clay and MPEG-based polycarboxylate superplasticizers, Cem. Concr. Res. 42 (2012) 847–854.
[42] D. Vrankovic, K. Wissel, M. Graczyk-Zajac, R. Riedel, Novel 3D Si/C/SiOC nanocomposites: toward electrochemically stable lithium storage in silicon, Solid State Ion. 302 (2017) 66–71.
[43] S. Martínez-Crespiera, E. Ionescu, H.-J. Kleebe, R. Riedel, Pressureless synthesis of fully dense and crack-free SiOC bulk ceramics via photo-crosslinking and pyrolysis of a polysiloxane, J. Eur. Ceram. Soc. 31 (2011) 913–919.
[44] A. Leenaars, K. Keizer, A. Burggraaf, The preparation and characterization of alumina membranes with ultra-fine pores, J. Mater. Sci. 19 (1984) 1077–1088.
[45] W.-W. Li, G.-P. Sheng, X.-W. Liu, H.-Q. Yu, Recent advances in the separators for microbial fuel cells, Bioresour. Technol. 102 (2011) 244–252.
[46] J. Winfield, L.D. Chambers, J. Rossiter, I. Ieropoulos, Comparing the short and long term stability of biodegradable, ceramic and cation exchange membranes in microbial fuel cells, Bioresour. Technol. 148 (2013) 480–486.
[47] M. Wilhelm, M. Adam, M. Bäumer, G. Grathwohl, Synthesis and properties of porous hybrid materials containing metallic nanoparticles, Adv. Eng. Mater. 10 (2008) 241–245.
[48] H. Xu, S. Tao, D. Jiang, Proton conduction in crystalline and porous covalent organic frameworks, Nat. Mater. 15 (2016) 722–726.
[49] L.-C. Jheng, S.L.-C. Hsu, T.-Y. Tsai, W.J.-Y. Chang, A novel asymmetric polybenzimidazole membrane for high temperature proton exchange membrane fuel cells, J. Mater. Chem. A 2 (2014) 4225–4233.
[50] H. Zhang, P.D.A. Nunes, M. Wilhelm, K. Rezwan, Hierarchically ordered micro/meso/macroporous polymer-derived ceramic monoliths fabricated by freeze-casting, J. Eur. Ceram. Soc. 36 (2016) 51–58.
[51] T. Prenzel, T. Guedes, F. Schlüter, M. Wilhelm, K. Rezwan, Tailoring surfaces of hybrid ceramics for gas adsorption–from alkanes to CO_2, Sep. Purif. Technol. 129 (2014) 80–89.
[52] K.M.S. Meera, R.M. Sankar, A. Murali, S.N. Jaisankar, A.B. Mandal, Sol–gel network silica/modified montmorillonite clay hybrid nanocomposites for hydrophobic surface coatings, Colloids Surf. B 90 (2012) 204–210.
[53] M. Rezaei-DashtArzhandi, A. Ismail, G. Bakeri, S. Hashemifard, T. Matsuura, Effect of hydrophobic montmorillonite (MMT) on PVDF and PEI hollow fiber membranes in gas–liquid contacting process: a comparative study, RSC Adv. 5 (2015) 103811–103821.
[54] R.-Y. Lin, B.-S. Chen, G.-L. Chen, J.-Y. Wu, H.-C. Chiu, S.-Y. Suen, Preparation of porous PMMA/Na+–montmorillonite cation-exchange membranes for cationic dye adsorption, J. Membr. Sci. 326 (2009) 117–129.
[55] E. Wang, B. Li, B. Zhang, Z. Wang, The proton conductivity of heteropoly compounds, Transit. Met. Chem. 22 (1997) 58–60.